

1
2
3
4 **Boxwork and ferromanganese coatings in hypogenic caves: an**
5 **example from Sima de la Higuera Cave (Murcia, SE Spain)**
6
7
8

9 Fernando Gázquez¹, José-María Calaforra^{1*}, Fernando Rull^{2,3}

10
11 ¹Water Resources and Environmental Geology Research Group – Dept. of Hydrogeology and Analytical
12 Chemistry - University of Almería, Crta.Sacramento s/n, 04120 La Cañada de San Urbano, Almería.
13 (f.gazquez@ual.es) (jmcalaforra@ual.es) * Corresponding author

14 ²Unidad Asociada UVA-CSIC al Centro de Astrobiología, University of Valladolid. Parque tecnológico
15 Boecillo, 47151. Valladolid (Spain) (rull@fmc.uva.es)

16 ³Centro de Astrobiología (CSIC-INTA). Crta. Ajalvir, 28850. Torrejón de Ardoz, Madrid (Spain)

17
18
19 **Abstract**
20

21
22 This paper examines the greyish-blue deposits that were recently discovered in the
23 lower levels of the Sima de la Higuera Cave (Murcia, SE Spain) which occur as patinas
24 over the walls and ceilings, as well as coating *boxwork* formations. Their mineralogy
25 was determined using XRD and micro-Raman spectroscopy, while EDX microanalysis
26 was used to determine their elemental composition. The mineralogical analyses revealed
27 the presence of Mn oxides (todorokite and pyrolusite) and Fe with a low degree of
28 crystallinity, whereas EDX microprobe showed elevated concentrations of Mn (38.2 %
29 wt), Fe (15.2 % wt) and Pb (8.1 % wt). The ferromanganese oxyhydroxides occur as
30 botryoidal aggregates overlying blades of calcite that have a visibly sugary texture. The
31 speleogenetic model proposed describes (1) an initial phase of precipitation of
32 hydrothermal calcite veins (of hypogenic origin) within the fissures of the host rock
33 under phreatic conditions and (2) a subsequent vadose phase involving preferential
34 corrosion of the carbonate host rock caused by lowering of the pH resulting from CO₂
35 diffusion in condensed water and oxidation of Fe and Mn under aerobic conditions,
36 probably mediated by microorganisms. It is this later phase that gave rise to the
37 *boxwork*. The *boxwork* of the Sima de la Higuera Cave is a singular example of a

38 formation that is generated by dissolution-corrosion of the rock due to acidification
39 caused by oxidation of iron and manganese.

40

41 **Keywords:** speleothems, ferromanganese oxyhydroxides, boxwork, hypogenic caves,
42 corrosion, Sima de la Higuera Cave.

43

44

45 **1. Introduction**

46

47 The mineralogy, chemistry and genetic aspects of the oxides and hydroxides of iron and
48 manganese speleothems have been extensively studied in many caves (Crabtree, 1962;
49 Moore, 1981; Gascoine, 1982; Hill, 1982; Kashima, 1983; Peck, 1986; Jones, 1992;
50 Onac, 1996, 1997; Northup et al., 2003; Spilde et al., 2006; White et al., 2009; Rossi et
51 al., 2010; Gázquez et al., 2011; Gázquez et al., 2012).

52 Manganese, soluble in its divalent form (Mn^{2+}) oxidises to trivalent (Mn^{3+}) or
53 tetravalent (Mn^{4+}) manganese in superficial environments and at low temperature, in a
54 process that is frequently attributed to bacterial mediation (Calvert and Pedersen, 1996;
55 Jürgensen et al., 2004). Microorganisms accelerate the rate of oxidation of Mn^{2+} by
56 several orders of magnitude with respect to abiotic catalysis, so it is accepted that the
57 precipitation of oxides of Mn^{3+} and Mn^{4+} depends on biological processes (Nealson et
58 al., 1988). This recognition has led to a number of investigations focusing on the role
59 played by microorganisms in precipitation of these oxides (Peck, 1986; Boston et al.,
60 2001; Spilde et al., 2005, 2006; Rossi et al., 2010).

61 Originally, it was thought that the ferromanganetic deposits were corrosion residues that
62 derived exclusively from dissolution of the carbonate substratum due to condensation
63 (Queen, 1994), or from acid corrosion in hypogenic caves (Davis, 2000; Provencio and
64 Polyak, 2001). However, recent work has proposed the source of Fe and Mn to be from
65 mobilization of these elements contained in mineralizations of the host rock (Gázquez et
66 al., 2011; Gázquez et al., 2012) or from dissolution of these elements in vadose parts of
67 the cave (Spilde et al., 2006). One way or the other, ferromanganetic speleothems in
68 caves tend to be of two distinct types:

69 (1) The first group consists of Fe-Mn minerals, usually with smooth surfaces, deposited
70 on the cave walls, floors and ceilings (Onac et al., 1996; White et al., 2009; Gázquez et
71 al., 2011). Sometimes, these types of crust are intercalated with detrital material or

72 “fossilized” inside carbonate speleothems (Peck, 1986; Provencio and Polyak, 2001;
73 Yusta et al., 2009; Gázquez et al., 2011). As a general rule, these ferromanganese
74 speleothems are usually deposited by moving water and the underlying substrate does
75 not appear to be weathered.

76 (2) The second group consists of precipitates that have the aspect of rough patinas
77 deposited over the cave walls and ceilings, usually on top of visibly altered carbonate
78 substrates, dubbed "punk rock" by Hill (1987). The presence of this type of
79 ferromanganese deposits is relatively scarce compared to the abundant crust deposits of
80 the first group and their origin seems to be linked to weathering of the host rock. The
81 most significant examples of this typology are found in hypogenic cave such as Spider
82 Cave and Lechuguilla Cave (Carlsbad Caverns National Park, New Mexico) (Davis,
83 2000; Provencio and Polyak, 2001; Northup et al., 2003; Spilder et al., 2005, 2006), in
84 Jewel Cave and Wind Cave (South Dakota) (Chelius and Moore, 2004; White et al.,
85 2009) and Cupp-Coutunn Cave (Turkmenistan) (Maltsev, 1997).

86 The present work studies a new example of this second group of ferromanganese
87 deposits, which has been recently discovered in the Sima de la Higuera Cave (Murcia,
88 Southeast Spain) (Ferrer, 2010), also of hypogenic origin. The mineralogical and
89 geochemical data obtained have enabled us to establish a scheme of evolution to
90 describe the genesis of this peculiar speleothem, based on corrosion of the host rock,
91 which in this case leads to the formation of unique *boxwork* coated with ferromanganese
92 oxyhydroxides. The term “*boxwork*” refers to mineral veins in the bedrock which, due
93 to the greater resistance of the calcite in these veins, protrude from the cave wall after
94 dissolution and/or corrosion of the surrounding host rock (Hill and Forti, 1997).

95

96 **2. Geological setting**

97

98 The Sima de la Higuera (Fig tree Cave) is located in the Sierra de Espuña, in the
99 municipal district of Pliego (Murcia Region). Its entrance lies 485 m a.s.l., crowned by a
100 large fig tree that gives the cave its name. Speleological exploration of the cave began
101 in 1997, although there is some evidence that it was discovered earlier than this date
102 (Club Cuatro Pico and Club Pliego Espuña, 2001; Ferrer, 2010). Its surveyed length is
103 around 5500 m and the maximum depth is 156 m below the cave entrance, and 82 m
104 below the base of the entrance sinkhole (Fig. 1B).

105 The cave lies in Oligo-Miocene detrital and marly limestone. Interlayered carbonate
106 conglomerate also appears below the -110 m level, where the ferromanganese deposits
107 studied in this work are emplaced. The carbonate sequence is quite fractured due to
108 NW-SE pressure that has given rise to a series of joints and faults that subsequently
109 determined the cave's morphology, particularly its deeper levels. Mineralizations of
110 metallic sulfides do not appear in the cave setting. In contrast, manganese minerals such
111 as pyrolusite, have been identified in the Tertiary carbonate sequence within the cave,
112 and also appear outside the cave. Significant hydrothermal springs arise in the vicinity
113 of the cave, with temperatures that range from 30 to 50 °C. These include those of Mula
114 and Archena, 10 and 20 km from the cave, respectively. The high heat flux is due to the
115 relative thinning of the earth's crust and the presence of recent magmatic masses
116 produced by volcanic eruptions that occurred a million years ago (Pinuaga-Espejel et
117 al., 2000).

118 The mouth of the cave gives access to a subvertical sinkhole 74 m deep, which is
119 developed along the length of a diaclase that runs E-W and finally opens out in the
120 Junction Chamber (Sala de la Unión). This chamber and the galleries that communicate
121 with it form one of the upper levels of the cave, which also run E-W. On this level
122 appear several, small hanging lakes (Coral Lake - Lago de los Corales, and the Bath
123 Chamber –Sala de la Bañera). Beyond this point, the cave morphology changes
124 considerably, with larger galleries and chambers, such as the Ghost Chamber (Sala de
125 los Fantasma) or Paradise Chamber (-95 m level, Sala Paraíso), which occupy an
126 intermediate level. Lastly, the deepest levels include labyrinthine galleries (three-
127 dimensional “*maze caves*”) that are smaller in size, and it is here where the
128 ferromanganese speleothems, which are the subject of this study, are found (Manganese
129 Gallery) (Fig. 1C).

130 The cave contains strong evidence of a hypogenic origin. In this study, we use the term
131 “hypogenic” as postulated by Palmer (2011), who suggested that hypogenic caves form
132 due to the upward flow of deep-seated water or by solutional aggressivity generated at
133 depths below the ground surface. In the Sima de la Higuera Cave the hypogenic
134 mechanism is evidenced by the presence of types of speleothems and geomorphological
135 features that are typically related to hypogenic caves such as calcite raft cones, tower
136 cones, mammillary crusts (cave clouds) and folia, specific corrosion forms, copula and
137 condensation domes, scallops, etc. (Audra et al., 2002, 2009; Klimchouk, 2009). The
138 location of these elements in the cross-section of the cave (Fig. 1C) suggests an upflow

139 of thermal water during the cave speleogenesis, as indicated in other hypogenic caves
140 (Audra et al., 2009).

141 In addition, its ambient temperature is elevated compared to the annual mean outside
142 temperature of 13.8 °C; the current cave temperature oscillates between 18.6 °C and
143 21.7 °C, increasing slightly in the deeper parts (Club Cuatro Pico and Club Pliego
144 Espuña, 2001) which indicates a significant positive thermal anomaly. Relative
145 humidity of the cave air is between 87.5 and 90 % (Club Cuatro Pico and Club Pliego
146 Espuña, 2001).

147 Although the evidence points to deep hydrothermal water flowing through the caves in
148 the past, present-day water inflow is entirely from infiltration of meteoric water. There
149 are only a few vadose speleothems generated from dripwater (stalactites, stalagmites,
150 etc.) in the shallowest levels, around -74 m, and above the level of the Bath Chamber.

151

152 **3. Materials and methods**

153 **3.1. Description of the samples**

154

155 The sample analysed consists of a fragment of a “*boxwork*” blade (SHG), taken from
156 the roof of the Manganese Gallery, situated in one of the deeper levels of Sima de la
157 Higuera Cave, at the -110 m level (Fig.1). The sample comprised a mineral lamina, 5-10
158 mm thick with a sugary texture, whose outer surface is covered by greyish-blue
159 deposits, rough in texture and dull (Fig. 2A, B).

160 In places, the *boxwork* projects from the cave wall more than 30 cm into the cave void
161 (Fig. 2D) and covers hundreds of meters of cave wall and ceiling, especially in the
162 galleries of the mid-lower levels of the cave. Nevertheless, the *boxwork* can also be
163 observed in shallower parts of the cave, though much of the time it is barely visible,
164 having been totally eroded away or widely covered by more recent speleothems, like
165 coralloids or *popcorn*.

166 In places, the dark deposits are accompanied by others, pink or reddish in colour (Fig.
167 2E) and, less frequently, these coloured patinas cover calcite spar, some of them
168 centimetric in size (Fig. 2B). In this case, the crystal surfaces are also rough, although
169 the crystal shapes are usually well preserved. In the deep galleries, there is also a
170 stratum of conglomerates whose pebbles are totally covered in a similar dark patina
171 (Fig. 2F,G).

172

173 3.2. Analytical methodology

174

175 SEM microphotographs were taken using a HITACHI S-3500 instrument in high
176 vacuum mode. The samples were previously dried and coated with graphite to increase
177 electron transmissivity. The elemental chemistry was determined by EDX (Energy
178 dispersive X-ray spectroscopy) microprobe at nine points with different typology over
179 the *boxwork* sample (Fig. 3). Semiquantitative EDX microanalyses (Energy dispersive
180 X-ray spectroscopy) used the same instrument coupled to an Oxford INCA 7210 X-ray
181 detector, using a voltage of 20 kV. The diameter of the beam was approximately 1 μm .
182 The limit of detection of this technique enables major elements such as Fe, Mn, O, Si,
183 Al, Ca, Mg, Pb and Ba to be analysed (Table 1). Carbon concentration was not
184 measured due to masking by the graphite coating.

185 A subsample of these dark materials was extracted using a needle for later mineralogical
186 analysis by XRD (X-ray diffraction). The mineralogy of the internal crystalline lamina
187 was also determined by XRD of a powdered sample. Mineral analysis using X-ray
188 diffraction (XRD) was done at ambient temperature in a single-crystal diffractometer
189 using a BRUKER APEX CCD area detector, modified for analysis of powdered
190 samples. $\text{MoK}\alpha$ cathode radiation was used ($\lambda = 0.71073 \text{ \AA}$) using the ω scanning
191 method, within angular limits $1.96 < \theta < 23.298$. This technique allows minimal
192 quantities of samples to be analysed ($< 0.05 \text{ mg}$) but carries the disadvantage of low
193 resolution in the resulting diffractograms.

194 The mineralogical nature of the two clearly differentiated zones was also studied *in situ*
195 by micro-Raman spectroscopy. The excitation source was a Laser Research Electro-
196 Optics (REO) working at 632.8 nm. The spectrometer used was a KOSI HoloSpec f/1.8i
197 model from Kaiser, with Rayleigh scattering of 633 nm, a spectral range of Raman
198 displacement of $0\text{-}3800 \text{ cm}^{-1}$ and spectral resolution of 5 cm^{-1} . The CCD used was a
199 DV420A-OE-130 model from Andor. The Raman head used was KOSI MKII, HFPH-
200 FC-S-632.8 model from Kaiser coupled by optical fibre. Microanalyses of up to 5 μm
201 diameter spot were undertaken with a Nikon Eclipse E600 microscope. The microscope
202 was coupled to the Raman probe and a JVC TK-C1381EG videocamera. For all of the
203 spectra, the laser power used on the sample was 15 mW, and the irradiance, 2.4 kW/cm^2
204 at 50X. This ensures no thermal damage to the samples. Acquisition time was 6 s and 5
205 accumulations were done. The sample was manually scanned, while the height of focus
206 was varied in order to optimize the intensity of the spectra signals. The spectra obtained

207 were compared with the RRUFF Raman mineralogical database standard
208 (<http://rruff.info/>) for calcite and Fe-Mn oxyhydroxides and our own database.

209

210 **4. Results**

211

212 The SEM microphotographs allowed two visibly different zones to be broadly identified
213 (Fig. 3A). The first comprises sub-millimetric euhedral calcite crystals, some of which
214 have a sphenoidal habit with well-defined faces and edges. Over this mineral lamina
215 appear botryoidal structures which, observed in BSE (Back-scatter electron imagery)
216 mode, show a lighter colouration than the underlying calcite crystals (Fig. 3B). This fact
217 suggests that the coating layer is composed of relatively heavier elements than those
218 comprising the hydrothermal calcite blades, which seems to be intensely altered,
219 particularly in the zones covered by these botryoidal features (Fig. 3C). The areas that
220 lack this covering also appear to have been altered, although to a lesser degree (Fig.
221 3D).

222 The morphology of the altered calcite varies from hexagonal or pseudo-hexagonal (Fig.
223 3F) to scalenohedral forms (Fig. 3H), aligned with the habit of the calcite crystals. In
224 the most altered zones, one is left with three-dimensional voids that also have a
225 hexagonal pattern (Fig. 3G). Within the cavities are filaments with a markedly biotic
226 aspect, which suggests that the cause of the alteration could be microbial activity (Fig.
227 3I).

228 The Raman spectroscopy identified that the dark botryoidal features that appears
229 partially covering calcite crystals are metallic oxides-hydroxides. The Raman signals
230 detected at 633 and 594 cm^{-1} are indicative of polymetallic oxides and/or hydroxides,
231 probably Fe-Mn minerals, which usually give Raman signals in this range (Dunn et al.,
232 2003; Mironova-Ulmane et al., 2009) (Fig. 4A). However, the precise mineralogy of
233 these substances could not be identified using this technique, since there was no
234 correspondence in the RUFF mineralogical database. The signal at 488 cm^{-1} was
235 assigned to the vibration of the Si-O-Si bonds that typifies clays (Frost, 1995). With
236 respect to the other Raman signals encountered, the well-defined bands at 1086, 711 and
237 281 cm^{-1} are evidence of the presence of calcite (Rutt and Nicola, 1974).

238 Lastly, the sugary-textured mineral substrate (Fig. 3D), over which the ferromanganese
239 deposits have developed, verified that it was calcite (Fig. 3C); it presented the typical

240 signals for this mineral at 1435, 1744, 1086, 711 and 281 cm^{-1} (Rutt and Nicola, 1974)
241 (Fig. 4B).
242 Additionally, mineral analysis of the same dark patina deposited over the *boxwork* (Fig.
243 3E) using X-ray diffraction found Mn phases to be present, including todorokite
244 ($\text{NaMn}_6\text{O}_{12}\cdot 3\text{H}_2\text{O}$) (22 %) and pyrolusite (MnO_2) (16 %). These minerals are in
245 addition to calcite (42 %) and amorphous phases (20 %), probably poorly crystalline Fe
246 oxides that were also confirmed using the EDX microprobe (Fig. 4 A).
247 The chemical composition of the patinas was determined by EDX microprobe at nine
248 points with differing typology found over *boxwork* from the Sima de la Higuera (Table
249 1). Although the percentage weight of Fe and Mn is relatively low in the total sample
250 (62 and 32 ppm, respectively, as determined by XRF), high concentrations of these
251 elements were detected using EDX microanalysis (Table 1), so corroborating the
252 mineralogic nature of these deposits. The points analysed over the botryoidal structures
253 (SHG-1, SHG-3 and SHG-6 in Fig. 3) revealed Mn concentrations ranging between
254 29.2 - 38.2 % wt. whereas Fe concentrations range between 10.3 - 15.2 % wt. There
255 were also relatively high concentrations of elements not detected in the underlying
256 calcite, such as Pb (up to 8.1 % wt.) and Ba (up to 2.7 % wt.).
257 The microanalyses done on the sugary-textured calcite show that the unaltered zones
258 (SHG-2, SHG-5 and SHG-9 in Fig. 3) contain low concentrations of Mn and Fe, below
259 2.8 and 1.5 % wt., respectively. The concentration of these elements over the zones of
260 altered calcite (SHG-4, SHG-7 and SHG-8 in Fig. 3) is similar to the unaltered zones
261 (without botryoidal features), falling below 1 and 2.2 % wt. for Mn and Fe, respectively.

262

263 **5. Discussion**

264

265 The Mn-Fe deposits in the Sima de la Higuera Cave have characteristics that are totally
266 different from those normally described in ferromanganese speleothems. In general, the
267 crusts reported in other caves have a plastic texture like a gel (Onac et al., 1997), or else
268 occur as laminae, frequently intercalated with detrital material (Rossi et al., 2010;
269 Gázquez et al., 2011); their origin is usually related to flowing water or alternating
270 vadose and phreatic conditions.

271 However, there is clear evidence that the Mn and Fe deposits of Sima de la Higuera
272 Cave have a completely different origin, starting with the striking arrangement of these

273 minerals in the deepest galleries of the cave. They commonly form a rough patina
274 coating the *boxwork* blades, whose structure is visibly altered and fragile.
275 This type of thin blades made of reticulate crystalline laminae (*boxwork*) has been
276 described in other caves (Hill and Forti, 1997). The genesis of the majority of these is
277 related to the infill of fractures in the host rock with minerals that are slightly more
278 resistant than the surrounding carbonate material, which are generally more readily
279 eroded by condensation-corrosion mechanisms (Palmer, 1981). Calcite veins
280 precipitated at low temperature are common (Hill and Forti, 1997), though some cases
281 have been reported where the infilled calcite has been precipitated from hydrothermal
282 water, as in the case of the *boxwork* in Wind Cave (South Dakota). There, the
283 temperature of formation of speleothems is estimated to have been 55 °C, based on
284 analysis of fluid inclusions in the *boxwork* veins (LaRock and Cunningham, 1995).
285 While, in the case of the *boxwork* from the Sima de la Higuera Cave, there is no
286 information about fluid inclusions, the phaneritic sugary texture of the calcite that
287 composes these blades, together with the great profusion of features that are typical of
288 hypogene speleogenesis (mammillary crusts, bubble trails, tower cones, folia, calcite
289 spar and others) suggest that these infills were precipitated under phreatic conditions
290 from thermal water in a subaqueous environment, prior to the *boxwork* formation. This
291 theory is also supported by the emplacement of spar-like and phaneritic calcite infills,
292 that occasionally reach centimetric dimensions (Fig. 2B), in the upper levels of the cave
293 and which, in other caves, have also been proposed as indicators of thermal conditions
294 prevailing during their genesis (Lundberg et al., 2000). Occasionally, the centimetric
295 calcite crystals of Sima de la Higuera Cave are also covered by rough greyish-blue
296 patinas. Nevertheless, these spar crystals are not totally dissolved like the submillimetric
297 crystals of the *boxwork* blades. Corrosion could affect both types of spar crystals
298 equally; however, this alteration is only visible at microscopic scale using SEM.
299 In places, the calcite veins are arranged in a three-dimensional network, which also
300 appears covered by ferromanganese oxyhydroxides. In this case, hydrothermal calcite
301 crystals were precipitated, infilling the abundant cracks of the bedrock that had been
302 previously fractured by tectonic forces (Figs. 5A, B). During a later stage, *boxwork* like
303 that of Fig. 2E formed under vadose conditions.
304 Subaerial condensation corrosion occurred after the cave drained. Condensation and
305 CO₂ diffusion in the condensed water are identified as being the precursor processes for
306 dissolution of the carbonate rock both in caves that were epigenic and non-thermal in

307 origin (Jameson, 1991; Tarhyle-Lips and Ford, 1998; Freitas and Shemekal, 2006), as
308 well as in hypogenic caves, exhibiting specific patterns of dissolution (Cigna and Forti,
309 1986; Bakalowicz et al., 1987; Sarbu and Lascu, 1997; Audra et al., 2007).

310 In the Sima de la Higuera Cave, the rising of hot air loaded with water vapour from the
311 deepest levels of the cave led to condensation over the walls of the Manganese Gallery,
312 whose temperature was slightly lower than that of the air rising from depth. This
313 dissolution process could have been enhanced as a consequence of the CO₂
314 concentration in the cave air. Currently, this concentration usually reaches 2000 ppm in
315 the lower and intermediate cave levels and it might have been greater in the past due to
316 degassing of hydrothermal water. This mechanism of CO₂ diffusion has also been
317 proposed as the precursor of corrosion of host rock in other thermal caves (Sarbu and
318 Lascu, 1997).

319 Nonetheless, current processes of condensation in Sima de la Higuera Cave do not seem
320 very active, particularly in the Manganese Gallery where there is no condensed water on
321 the gallery walls and relative humidity is below 90 % (Club Cuatro Pico and Club
322 Pliego-España, 2001). The great profusion of Fe-Mn oxyhydroxides coating the gallery
323 surfaces suggests that corrosion of the host rock and of the hydrothermal calcite blades
324 themselves could have been due to oxidation of Fe²⁺ and Mn²⁺ that were precipitated as
325 ferromanganese oxyhydroxides.

326 From this perspective, the “in situ” dissolution processes of the host rock, which could
327 contain the Fe and Mn in their reduced form, would involve oxidation of these as they
328 came into contact with the cave atmosphere, and they would remain attached to the
329 bedrock surfaces (Cunningham et al., 2005). Although iron and manganese are elements
330 that are frequently found as co-precipitates of marine carbonates (Morse and McKenzie,
331 1990), other studies have highlighted that the volume of manganese and iron usually
332 precipitated in this type of crust is much greater than could have come from “in situ”
333 dissolution of the host rock (Spilde et al., 2005). This imbalance is even more striking in
334 cases where the profusion of ferromanganese structures is so spectacular, such as in
335 Lechuguilla Cave (Davis, 2000) or in the current case of the Sima de la Higuera Cave.

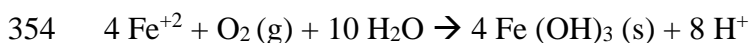
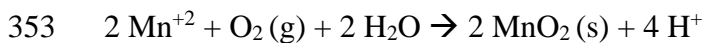
336 The significant quantities of the iron and manganese precipitates in these caves may
337 have derived from dissolution of the host rock overlying these galleries.

338 Thus, manganese and iron could be mobilized in the vadose zone by dissolution of the
339 Oligocene-Miocene carbonate enclosing the cave. In fact, manganese minerals, such as
340 pyrolusite, appear in the Tertiary carbonate sequence in which the cave is developed. It

341 is likely that dissolution of these metallic oxides under anoxic conditions could liberate
342 these elements in their reduced forms (Mn^{2+} and Fe^{2+}). Subsequently, metals were
343 carried by flowing water through fractures, and even through the intercrystalline pores
344 of the hydrothermal calcite veins. Eventually, the solution reached the cave where
345 metals oxidized under subaerial conditions (Fig. 5D).

346 The process of oxidation of these metals is frequently mediated by microorganisms that
347 use reduced manganese and iron (Mn^{2+} and Fe^{2+}) as their energy source (Nealson et al.,
348 1988; Spilde et al., 2005) (Fig. 5D). Microorganisms in the Fe-Mn crusts of Sima de la
349 Higuera Cave have been detected in various voids, where one can observe intricate
350 bacterial filaments that are probably linked to the oxidation of Fe and Mn, according to
351 the reactions:

352



355

356 As can be deduced from these chemical transformations, oxidation of manganese and
357 iron gives rise to protons that acidify the medium, and so lead to corrosion of the calcite
358 beneath. In this way, formation of *boxwork* is encouraged by preferential dissolution of
359 the microcrystalline host rock, which is more soluble than the blades of sugary-textured
360 hydrothermal calcite.

361 On the other hand, the calcite veins that remain exposed are also affected by corrosion
362 caused by the oxidation of the iron and manganese and CO_2 diffusion in condensed
363 water, as seen in Fig. 3, where calcite "ghosts" (molds around former calcite) can also
364 be seen either with a pseudo-hexagonal (Fig. 3C) or scalenohedral (Fig. 3H) structure,
365 depending on the degree of corrosion. The scalenohedral forms appear in the less
366 corroded areas, frequently on the faces of the rhombohedral calcite $\{10\bar{1}4\}$ (Fig. 3H).
367 The same pattern has been observed on a microscopic scale in experiments relating to
368 the initial phases of superficial dissolution of calcite (Astilleros et al., 2008). The initial
369 phases of dissolution by corrosion are characterized by regression of the exfoliation
370 laminae and by generation and enlargement of dissolution pits, which have a
371 characteristic rhomboid form with sides parallel to the direction $\langle\bar{4}41\rangle$ (Astilleros et al.,
372 2008). They ultimately result in the scalenohedral corrosion forms that are visible on the
373 crusts. On the other hand, the pseudo-hexagonal "ghosts" of formed calcite appear as
374 reticules over the surface of the crusts in areas where there is a higher density of

375 botryoidal Fe-Mn precipitates (Fig. 3C). On other occasions, the pseudo-hexagonal
376 morphology appears in tridimensional structures generated by the dissolution of the
377 preceding calcite crystals (Fig. 3G). In both cases, the hexagonal morphology seems to
378 be related to a more advanced phase of calcite corrosion. Differences in the magnitude
379 of the condensation mechanism at microscopic scale could have played a significant
380 role in the differential dissolution-corrosion pattern of the calcite blades.

381

382 **6. Conclusions**

383

384 Two stages can be differentiated during the genesis of the ferromanganese *boxwork* in
385 the Sima de la Higuera Cave: (1) precipitation of sparitic calcite veins in the fissures of
386 the carbonate host rock when the cave was submerged in the thermal aquifer water; and
387 (2) corrosion of carbonates by acid generated due to CO₂ diffusion in condensed water
388 and oxidation of reduced Fe-Mn in aerobic conditions. The acid attack preferentially
389 dissolved the carbonate host rock, which has a microcrystalline structure, while the
390 veins of sparitic calcite, precipitated in earlier phases, present greater resistance to
391 corrosion. In this way, the calcite blades projected into the cave in the form of a
392 *boxwork*.

393 The *boxwork* in the Sima de la Higuera Cave is a singular example of structures
394 generated by dissolution-corrosion of the rock due to acidification resulting from the
395 diffusion of CO₂ in the cave atmosphere and most probably as a consequence of
396 oxidation of iron and manganese by microorganisms.

397

398 **Acknowledgements**

399

400 The authors are grateful for the support of Esmeralda Urea and Sonia Mañas, SEM and
401 XRD facilities of the Servicios Centrales de Investigación of the University of Almería.
402 We are also grateful to Aurelio Sanz, the technician who performed the Raman analyses.
403 Financial support was made available through the Spanish Science Grant AP-2007-
404 02799, the funds of the Water Resources and Environmental Geology Research Group
405 (University of Almería) and the Project “RLS Exomars Science” (Ministry of Science
406 and Innovation, Spain and FEDER funds of EU). The authors thank Víctor Ferrer for his
407 kind permission to use photographs to illustrate this paper. The topography that appears
408 in this paper is courtesy of the Cuatro Picos Espeleo-Club (Cartagena) and the Pliego-

409 España Espeleo-Club (Pliego). The authors are grateful for the support of Andrés Ros
410 and Pepe Liza during the field work. Sarah Steines is also greatly acknowledged for
411 improving our English. Finally, the authors appreciate the suggestions made by two
412 anonymous reviewers, which helped to improve the original manuscript.

413

414 **References**

415

416 Astilleros, J.M., Sánchez-Pastor, N., Fernández-Díaz, L., 2002. La reactividad de las
417 superficies minerales en contacto con soluciones acuosas. *Macla* 8, 4-16.

418 Audra, Ph., Bigot, J.Y., Mocochain, L., 2002. Hypogenic caves in Provence (France).
419 Specific features and sediments. *Acta Carsologica* 31, 33-50.

420 Audra, Ph., Hoblea, F., Bigot, J.Y., Nobécourt, J.C., 2007. The role of condensation in
421 thermal speleogenesis: Study of a hypogenic sulfidic cave in Aix-les-Bains,
422 France. *Acta Carsologica* 36, 185-194.

423 Audra, Ph., Mocochain, L., Bigot, J.Y., Nobécourt, J.C., 2009. The association between
424 bubble trails and folia: a morphological and sedimentary indicator of hypogenic
425 speleogenesis by degassing, example from Adaouste Cave (Provence, France). *Int.*
426 *J. Speleol.* 38, 93-102.

427 Bakalowicz, W.J., Ford, D.C., Miller, T.E., Palmer, A.N., Palmer, M.V., 1987. Thermal
428 genesis of dissolution caves in the Black Hills, South Dakota. *Geol. Soc. Am.*
429 *Bull.* 99, 729-738.

430 Boston, P.J., Spilde, M.N., Northup, D.E. Melim, L.A., Sorok, D.S., Kleina, L.G.,
431 Lavoie, K.H., Hose, L.D., Mallory, L.M., Dahm, C.N., Crossey, L. J., Schelble,
432 R.T., 2001. Cave Biosignature Suites: Microbes, Minerals, and Mars.
433 *Astrobiology* 1, 25-54.

434 Calvert, S.E., Pedersen, T.F., 1996. Sedimentary geochemistry of manganese;
435 implications for the environment of formation of manganiferous black shales.
436 *Econ. Geol.* 91, 36-47.

437 Chelius, M.K., Moore, J.C., 2004. Molecular Phylogenetic Analysis of Archaea and
438 Bacteria in Wind Cave, South Dakota: *Geomicrobiol. J.* 21, 123–134.

439 Cigna, A.A., Forti, P., 1986. The speleogenetic role of airflow caused by convection. 1st
440 contribution. *Int. J. Speleol.* 15, 41-52.

441 Club Cuatro Pico, Club Pliego España, 2001. Sima de la Higuera. El mayor complejo
442 subterráneo topografiado de la Región de Murcia. *Subterránea* 16, 35-41.

- 443 Crabtree, P.W., 1962. Bog ore from Black Reef Cave. *Cave Science* 4, 360-361.
- 444 Cunningham, K.I., Northup, D.E., Pollastro, R.M., Wright, W.G., LaRock, E.J., 1995.
445 Bacteria, fungi and biokarst in Lechuguilla Cave, Carlsbad Caverns National
446 Park, New Mexico. *Environ. Geol.* 25, 2-8.
- 447 Davis, D.G., 2000. Extraordinary features of Lechuguilla Cave, Guadalupe Mountains.
448 *J. Cave Karst Stud.* 62, 147-157.
- 449 Dunn, D. S., Bogart, M. B., Brossiaand, C. S., Cragnoilino, G. A., 2000. Corrosion of
450 iron under alternate wet and dry conditions. *Corrosion* 56, 470–488.
- 451 Ferrer, V., 2010. *La Sima de la Higuera (Pliego-Murcia)*. 80 pp.
- 452 Freitas, C.R., Schmekal, A., 2006. Studies of corrosion/condensation process in the
453 Glowworm Cave, New Zealand. *Int. J. Speleol.* 35, 75-81.
- 454 Frost, R.L., 1995. Fourier Transform Raman Spectroscopy of Kaolinite, Dickite and
455 Halloysite. *Clays Clay Miner.* 43, 191-195.
- 456 Gascoine, W., 1982. The formation of black deposits in some caves of south east Wales.
457 *Cave Science* 9, 167-175.
- 458 Gázquez, F., Calaforra, J.M., Forti, P., 2011. Black Mn-Fe Crusts as Markers of Abrupt
459 Palaeoenvironmental Changes in El Soplao Cave (Cantabria, Spain). *Int. J.*
460 *Speleol.* 40, 163-169.
- 461 Gázquez, F., Calaforra, J.M., Forti, P., Rull, F., Martínez-Frías, J., 2012. Gypsum-
462 carbonate speleothems from Cueva de las Espadas (Naica mine, Mexico):
463 mineralogy and palaeohydrogeological implications. *Int. J. Speleol.* 41, 211-220.
- 464 Hill, C.A., 1982. Origin of black deposits in caves. *Natl. Speleol. Soc. Bull.* 44, 15-19.
- 465 Hill, C.A., 1987. *Geology of Carlsbad Cavern and other caves in the Guadalupe*
466 *Mountains, New Mexico and Texas: Socorro, NM, New Mexico Bureau of Mines*
467 *and Mineral Resources Bulletin* 117, 150.
- 468 Hill, C.A., Forti, P., 1997. *Cave minerals of the World 2*. National Speleological
469 Society, Huntsville. 461 pp.
- 470 Jameson, R.A., 1991. Features of condensation corrosion in caves of the Greenbrier
471 karst, West Virginia. *Natl. Speleol. Soc. Bull.* 53, 44.
- 472 Jones, B., 1992. Manganese precipitates in the karst terrain of Grand Cayman, British
473 West Indies. *Can. J. Earth Sci.* 29, 1125-1139.
- 474 Jürgensen, A., Widmeyer, J.R., Gordon, R.A., Bendell-Young, L.I., Moore, M.M.
475 Crozier, E.D., 2004. The structure of the manganese oxide on the sheath of the
476 bacterium *Leptothrix discophora*: An XAFS study. *Am. Mineral.* 89, 1110-1118.

- 477 Kampschuur, W., Langeberg, C.W., Montenat, Ch., Pignatelli, R., Egeler, C.G., 1972.
478 Mapa Geológico de España 1:50.000, hoja nº 933 (Alcantarilla). IGME, Madrid.
- 479 Khashima, N., 1983. On the Wad-minerals from the cavern environment. *Int. J. Speleol.*
480 13, 67-72.
- 481 Klimchouk, A. B., 2007. Hypogene Speleogenesis: Hydrogeological and
482 Morphogenetic Perspective. Special Paper no. 1, National Cave and Karst
483 Research Institute, Carlsbad, NM, 106.
- 484 Klimchouk, A.B., 2009. Morphogenesis of hypogenic caves. *Geomorphology* 106, 100-
485 117.
- 486 LaRock, E.J., Cunningham, K.I., 1995. Helictite bush formation and aquifer cooling in
487 Wind Cave, Wind Cave National Park, South Dakota. *Natl. Speleol. Soc. Bull.*
488 57, 43-51.
- 489 Lundberg, J., Ford, D.C., Hill, C.A., 2000. A preliminary U-Pb date on cave spar, Big
490 Canyon, Guadalupe Mountains, New Mexico. *J. Cave Karst Stud.* 62, 144-148.
- 491 Maltsev, V.A., 1997. Minerals of Cupp-Coutunn cave. In: *Cave Minerals of TheWorld*,
492 2nd edition. Huntsville, AL: *Natl. Speleol. Soc.* pp 323–328.
- 493 Mironova-Ulmanea, N., Kuzmina, A., Grube, M., 2009. Raman and infrared
494 spectromicroscopy of manganese oxides. *J. Alloys Compd.* 480, 97–99.
- 495 Moore, G.W., 1981. Origin of black deposits in caves. *Proceedings 8th International*
496 *Congress of Speleology, Bowling Green I and II:* 642-644.
- 497 Morse, J.W., MacKenzie, F.T., 1990. *Geochemistry of Sedimentary Carbonates.*
498 Elsevier. Amsterdam.
- 499 Nealson, K. H., Tebo, B. M., Rosson, R. A., 1988. Occurrence and mechanisms of
500 microbial oxidation of manganese. *Adv. Appl. Microbiol.* 33, 279–318.
- 501 Northup, D. E., Barns, S.M., Yu, L.E., Spilde, M.N., Schelble, R.T., Dano, K.E.,
502 Crossey, L.J., Connolly, C.A., Boston, J., Dahm, C.N., 2003. Diverse microbial
503 communities inhabiting ferromanganese deposit in Lechuguilla and Spider
504 Caves. *Environ. Microbiol.* 5, 1071-1086.
- 505 Onac, B.P., 1996. Mineralogy of speleothems from caves in the Padurea Craiului
506 Mountains (Romania), and their palaeoclimatic significance. *Cave Karst Sci.* 23,
507 109-124.

- 508 Onac, B.P., Pedersen, R.B., Tysseland, M., 1997. Presence of rare-earth elements in
509 black ferromanganese coating from Vântuliu cave (Romania). *J. Cave Karst Stud.*
510 59, 128-131.
- 511 Palmer, A.N., 1981. *Geology of Wind Cave, Wind Cave National Park, South Dakota:*
512 *Hot Springs, South Dakota. Wind Cave National History Association. 44 pp.*
- 513 Palmer, A.N., 2011. Distinction between epigenic and hypogenic caves.
514 *Geomorphology* 134, 9-22.
- 515 Peck, S.B., 1986. Bacterial deposition of iron and manganese oxides in North American
516 caves. *Natl. Speleol. Soc. Bull.* 48, 26-30.
- 517 Pinuaga-Espejel, J.I., Martínez Parra, M., González Casal, I., 2000. Potencial
518 hidromineral de la Región de Murcia. In: *Panorama actual de las aguas minerales*
519 *y Mineromedicinales en España, Madrid. pp. 361-373.*
- 520 Provencio, P.P., Polyak, V.J., 2001. Iron Oxide-Rock Filaments: Possible Fossil Bacteria
521 in Lechuguilla Cave, New Mexico. *Geomicrobiol. J.* 18, 297.
- 522 Queen, J.M., 1994. Influence of thermal atmospheric convection on the nature and
523 distribution of microbiota in caves environments. In: Sasowsky, I.D. and Palmer,
524 M.V., eds. *Breakthroughs in Karst Geomicrobiology and Redox Geochemistry,*
525 *Charles Town, WV:, Karst Waters Institute Special Publication Number 1, pp. 13-*
526 *14.*
- 527 Rossi, C., Lozano, R.P., Isanta, N., Hellstrom, J., 2010. Manganese stromatolites in
528 caves: El Soplao (Cantabria). *Geology* 38, 1119-1122.
- 529 Rutt, H. N., Nicola, J. H., 1974. Raman spectra of carbonates of calcite structure. *J.*
530 *Phys. C Solid State* 7, 4522.
- 531 Sarbu, S.M., Lascu, C., 1997. Condensation Corrosion in Movile Cave, Romania. *J.*
532 *Cave Karst Stud.* 59, 99-102.
- 533 Spilde, M.N., Northup, D.E. Boston, P.J., Schelble, R.T., Dano, K.E., Crossey, L.J.,
534 Dahm, C.N., 2005. Geomicrobiology of cave ferromanganese deposits: A field
535 and laboratory investigation. *Geomicrobiol. J. B* 22, 99–116.
- 536 Spilde, M.N., Northup, D.E., Boston, P., 2006. Ferromanganese deposits in the caves of
537 the Guadalupe Mountains. *New Mexico Geological Society Guidebook, 57th Field*
538 *Conference, Caves and Karst of Southeastern New Mexico, pp. 161-166.*
- 539 Tarhule-Lips, R.F.A., Ford, D.C., 1998. Condensation Corrosion in Caves on Cayman
540 Brac and Isla de Mona. *J. Cave Karst Stud.* 60, 84-95.

541 White, W.B., Vito, C., Scheetz, B.E., 2009. The mineralogy and trace element chemistry
542 of black manganese oxide deposits from caves. *J. Cave Karst Stud.* 71, 136-143.
543 Yusta, I., Castellano, A., Aranburu, A., Velasco, F., 2009. Los depósitos de Mn-Al-Fe de
544 la Cueva de Lazalday (Zarate, Alava): composición química y mineralogía.
545 *Geogaceta* 47, 117-120.
546 [http://rruff info/](http://rruff.info/) Ruff Mineralogical database. Accessed 10 May 2012

547
548

549 **FIGURE CAPTIONS**

550

551 **Figure 1.** A. Location and geological setting of the Sima de la Higuera Cave.
552 Geological cartography modified from Kampschuur et al., (1972); B. Plan view of its
553 development. The red circle indicates the location of the Manganese Gallery where the
554 *boxwork* sample was collected. Cave topography courtesy of the Speleological Clubs:
555 Cuatro Picos (Cartagena) and Pliego-Espuña (Pliego) (2001); C. Idealized cross section
556 and location of the main hypogenic geomorphological features and speleothem
557 formations in the Sima de la Higuera Cave. The red frame indicates the location of the
558 Manganese Gallery.

559

560 **Figure 2.** Hypogene ferromanganese *boxwork* from the Sima de la Higuera Cave
561 (Murcia): A. Manganese Gallery where it appears the ferromanganese *boxwork* studied
562 in this work. The lower parts of the gallery walls are covered by clayey minerals that
563 indicate a past water level. The ferromanganese oxyhydroxides also appear under these
564 detrital deposits; B. Ferromanganese *boxwork* on the ceiling of the Manganese Gallery
565 (-110 m); C. Calcite “spar” coating the cave walls beyond the “Bath Chamber”; D.
566 Ferromanganese *boxwork* on the ceiling of the Manganese Gallery, partially covered
567 with “popcorn”; E. Ferromanganese *boxwork* covered with coralloids; F, G. Clastic
568 materials covered with ferromanganese oxyhydroxides and desiccation mud crust on the
569 gallery floor; H. Large hydrothermal calcite veins filling fractures in the host rock
570 which origin is related to the mechanisms that generated the *boxwork* (Photos: Victor
571 Ferrer).

572

573 **Figure 3.** Secondary electron images of the manganese coatings on the *boxwork* of the
574 Manganese Gallery: A. General view where it appears calcite euhedral crystals covered

575 by ferromanganese patinas; B. BSE (Back-scatter electrons) image showing zones of
576 contrasting compositions. Clearer colour zones indicate Fe-Mn coatings while darker
577 colour areas are composed of altered euhedral calcite crystals; C. Fe-Mn oxyhydroxides
578 forming botryoidal structures over the visibly altered calcite substrate; D. Altered
579 sugary-textured calcite substrate; E. Detail of the botryoidal features made of
580 mineralizations of Fe-Mn oxyhydroxides; F. Details of the pseudo-hexagonal calcite
581 “ghosts” related to the alteration caused by oxidation of Fe and Mn; G. Three-
582 dimensional calcite “ghosts”; H. Scalenohedral calcite with molds; I. Biotic filaments
583 inside the corrosion cavities. Note that the numbers indicate the location of the EDX
584 microanalyses, whose results are summarised in Table 1.

585

586 **Figure 4.** Raman and EDX spectra of the Mn-Fe coatings from the Sima de la Higuera
587 Cave: A. Raman spectrum and EDX spectrum of the Mn-Fe oxyhydroxides coating; B.
588 Raman spectrum and EDX spectrum of the calcite blade substrate.

589

590 **Figure 5.** Genesis of the ferromanganese *boxwork* of the Sima de la Higuera: A.
591 Karstification and initial hypogene speleogenesis linked to hydrothermal water rising.
592 The cracks were enlarged by the hot water. Red = thermal water; B. Precipitation of
593 “spar” crystals of hydrothermal calcite filling host rock fractures by means diminishing
594 temperature. Yellow blocky pattern = calcite spar veins; C. Increasing cracks and voids
595 formation due to hydrothermal flow. Dissolution of the carbonate host rock in
596 underwater conditions and mobilization of Mn and Fe in their reduced forms; D. Walls
597 and ceiling dissolution/corrosion under vadose conditions. Mn^{2+} and Fe^{2+} from the
598 bedrock, both “in situ” and transported by flowing water coming from the vadose zone
599 were oxidized when reached the cave (dark blue line = ferromanganese oxyhydroxides),
600 probably via microbial activity in oxygenic environment. This reaction produces H^+ and
601 pH lowering conducting to calcite corrosion. CO_2 diffusion in condensed water could
602 also lead to acid corrosion. In places, clayey coatings and desiccation mud crusts appear
603 on the floor of the Manganese Gallery.

604

605 **Table 1.** Analysis of major elements. Analytical error ranges from ± 0.33 wt% for
606 oxygen to ± 0.13 wt% for aluminum. Error in Fe and Mn measurements was ± 0.2 wt%.
607 The location of the microanalysis samples is given in Fig. 3.

608